Catalysis Science & Technology

ROYAL SOCIETY OF CHEMISTRY

PAPER

View Article Online
View Journal | View Issue

Cite this: *Catal. Sci. Technol.*, 2020, **10**, 7186

Oxidative dehydrogenation of propane on silica-supported vanadyl sites promoted with sodium metavanadate†

Manouchehr Nadjafi, [a] Agnieszka M. Kierzkowska, [a] Paula M. Abdala, [a] Rene Verel, [b] Olga V. Safonova, [c] Alexey Fedorov *[a] and Christoph R. Müller *[a]

Received 19th June 2020,
Accepted 7th September 2020

DOI: 10.1039/d0cy01234c

rsc.li/catalysis

The promotion of silica-supported vanadyl species $[VO_4]/SiO_2$ (**1**) by α-$NaVO_3$ or β-$NaVO_3$ enhances the specific rate of the propene formation in oxidative dehydrogenation of propane (ODP) by, respectively, 30 and 125% at 450 °C and *ca.* 1 V nm^{-2} nominal coverage. The increased rate of propene formation is offset only moderately by a decreased selectivity to propene, which declines by 10 and 15% relative to **1** (74%) in α-$NaVO_3$/**1** and β-$NaVO_3$/**1**, at 5.8 and 8.2% propane conversion. The structural characterization of the promoted catalysts by Raman mapping, X-ray absorption near edge structure (XANES), transmission electron microscopy (TEM) and solid-state nuclear magnetic resonance (^{51}V and ^{23}Na MAS NMR) allowed for associating the higher specific activity of β-$NaVO_3$/**1** with a higher dispersion of vanadium sites on the silica support, while the agglomeration of these sites with the concomitant formation of a poorly dispersed $Na_{1+x}V_3O_8$ phase is related to a decreased catalytic activity. Surprisingly, solid-state ^{51}V NMR and Raman spectroscopies reveal that the α-$NaVO_3$/**1** and β-$NaVO_3$/**1** catalysts contain the metastable β-$NaVO_3$ phase, explained by a more favorable interaction of $Na_{1+x}V_3O_8/SiO_2$, formed after calcination in both materials, with β-$NaVO_3$ than with α-$NaVO_3$.

Introduction

Propene, a fundamental building block in the production of bulk chemicals and polymers,[1] is typically obtained as a byproduct from fluid catalytic cracking (FCC) and steam cracking of naphtha.[2] However, the ongoing replacement of naphtha by shale gas[3] decreases the propene production through this route, which occurs simultaneously with a growing demand for propene.[3,4] Industrial, "on-purpose" propene production technologies *via* propane dehydrogenation (PDH) rely currently on CrO_x/Al_2O_3 or Pt–Sn/Al_2O_3, both catalysts promoted with Na/K (Catofin and Oleflex processes, respectively).[5] These technologies have drawbacks, including coking, high energy demand ($\Delta H^{\circ}_{298K} = 124.6$ kJ mol^{-1}), low conversions (at the thermodynamic equilibrium, 25% at 527 °C), high price of Pt, and toxicity of Cr^{VI}.[2,5–7] An alternative to PDH is the oxidative dehydrogenation of propane (ODP) that exothermally converts propane and oxygen to propene and water ($\Delta H^{\circ}_{298K} = -177$ kJ mol^{-1}) at lower temperatures (*ca.* 450 °C). Propane conversion is not limited by thermodynamics in ODP and coking is avoided due to the use of oxygen, thus providing usually a stable catalytic performance. Despite its potential, no ODP process has yet been industrialized, primarily because of the insufficient selectivity to propene at high propane conversions.[6]

At low vanadium loadings (such as those used in this work), dehydrated vanadia on oxide supports features mostly site-isolated, surface-grafted tripodal vanadium oxo sites, $(-O)_3V{=}O$, often denoted $[VO_4]$ sites.[8–20] These species are among the best-performing ODP catalysts.[2,6,8,21,22] Alkali dopants were reported to improve propene selectivity of supported VO_x catalysts, which was, however, associated with a lower catalytic activity than in the undoped catalysts.[23,24] It was argued that the basic alkali doping decreased the strong acidity of the undoped catalysts,[23–25] in addition to weakening the V=O bond.[24,26] Furthermore, Na doping can improve the dispersion of VO_x sites on a silica support by increasing the reactivity of surface OH groups of the silica support.[26–28]

Recently, we have shown that a catalyst derived from silica supported sodium decavanadate ($Na_6V_{10}O_{28}$) provides 65%

[a] *Department of Mechanical and Process Engineering, ETH Zürich, Leonhardstrasse 21, CH-8092 Zürich, Switzerland. E-mail: fedoroal@ethz.ch, muelchri@ethz.ch*
[b] *Department of Chemistry and Applied Biosciences, ETH Zürich, Vladimir-Prelog-Weg 1-5, CH-8093 Zürich, Switzerland*
[c] *Paul Scherrer Institute, CH-5232 Villigen, Switzerland*

† Electronic supplementary information (ESI) available: Experimental details, XRD, NMR, Raman, H_2 temperature programmed reduction (TPR), XAS, DSC, and TEM data. See DOI: 10.1039/d0cy01234c

selectivity to propene at 6% propane conversion at 450 °C.[29] When heated under air to 600 °C, $Na_6V_{10}O_{28}$ decomposes on the silica surface to the metastable β-$NaVO_3$ phase along with a $Na_{1+x}V_3O_8$ phase interacting with the silica support ($Na_{1+x}V_3O_8/SiO_2$). The formation of β-$NaVO_3$ in the calcined $Na_6V_{10}O_{28}/SiO_2$ material under these conditions was surprising because the transformation of bulk and silica-supported β-$NaVO_3$ to α-$NaVO_3$ proceeds at notably lower temperatures than 600 °C and therefore an α-$NaVO_3$ phase would have been expected.[30,31] The presence of β-$NaVO_3$ in the calcined $Na_6V_{10}O_{28}/SiO_2$ suggests that $Na_{1+x}V_3O_8/SiO_2$ plays a role in stabilizing β-$NaVO_3$.[29]

With the objective of improving our understanding of the interaction between the $NaVO_3$ phases and the vanadyl sites on the silica surface, we incipient wetness impregnated (IWI) an aqueous solution of either α-$NaVO_3$ or β-$NaVO_3$ onto a SiO_2 support, followed by overnight drying at 100 °C and an IWI of an aqueous solution of NH_4VO_3. This procedure gave, after calcination, α-$NaVO_3$/**1** and β-$NaVO_3$/**1** materials with a similar nominal vanadium loading of *ca.* 1 V nm^{-2} and a Na/V ratio of *ca.* 0.6. We find that the phase of the $NaVO_3$ promoter used for the impregnation influences the increase of the initial specific rate for propene formation of the reference catalyst **1**, *i.e.* an increase by 30 and 125% is observed, respectively, for α-$NaVO_3$/**1** and β-$NaVO_3$/**1**. Interestingly, solid state ^{51}V NMR and Raman spectroscopy suggest that α-$NaVO_3$/**1** and β-$NaVO_3$/**1** contain the metastable β-$NaVO_3$ phase. Yet the catalytic activity of α-$NaVO_3$/**1** and β-$NaVO_3$/**1** and their deactivation with time on stream (TOS) are different, with the rate of propene formation decreasing after 4 h by 12 and 21%, respectively. Agglomeration of Na and V species in the used catalyst was identified as the driving force for the deactivation. We explain the higher activity of β-$NaVO_3$/**1** compared to α-$NaVO_3$/**1** by the higher dispersion of β-$NaVO_3$-$Na_{1+x}V_3O_8$/SiO_2 species in β-$NaVO_3$/**1** (Scheme 1).[6,20,32]

Results and discussion

Incipient wetness impregnation of ammonium metavanadate[6,8] was used to prepare $[VO_4]/SiO_2$ (**1**, 2.1 wt% V by ICP, Table S1†) containing *ca.* 1 V nm^{-2}, which is below the monolayer coverage for SiO_2 support.[17] Vanadyl sites on silica have been characterized in details in previous reports.[13,14,17,28,29,33–36] Since the nature of the supported VO_x species changes with hydroxylation of the support,[17,32,33] the materials discussed below were treated under synthetic air (500 °C, 1 h, 30 ml min^{-1}) and stored in a glovebox (H_2O and O_2 < 0.5 ppm), indicated by the respective subscript notation, for instance **1**$_{(500\text{-air})}$. To prepare α-$NaVO_3$/**1** and β-$NaVO_3$/**1** materials, silica was impregnated first with aqueous solutions of α-$NaVO_3$ or β-$NaVO_3$ (0.6 V nm^{-2}) followed by overnight drying at 100 °C and a subsequent IWI of NH_4VO_3 (0.4 V nm^{-2}). Calcined α-$NaVO_3$/**1** and β-$NaVO_3$/**1** contained 1.9 and 2.0 wt% of vanadium and a molar ratio of Na/V of 0.63 and 0.62 (by ICP), respectively, corresponding to a nominal silica coverage of *ca.* 1 V nm^{-2}. Although the nominal vanadium loading of the as impregnated α- and β-$NaVO_3$ promoted catalysts were similar to that of the benchmark catalyst (1 V nm^{-2}, *ca.* 2 wt%), the surface density of V calculated from the ICP-determined V loading and the specific surface area of the material (according to BET N_2 physisorption measurements) was notably higher for the promoted catalysts compared to **1** (*i.e.* 1.6 and 2.0 V nm^{-2} *vs.* 1.1 V nm^{-2}, see Table S1,† entries 1–4). This is explained by a reduced surface area of the silica support due to the etching effect caused by Na-containing precursors.[25] We have therefore optimized the loading of vanadium precursors in order to obtain a comparable surface density of V in the promoted catalysts and in **1**. This was achieved for α- and β-$NaVO_3$ promoted catalysts with a lower nominal vanadium loading (*i.e.* 0.7 V nm^{-2}, denoted in a subscript), resulting in 1.2 and 1.0 V nm^{-2}, respectively, after the calcination (Table S1,† entries 5–6). Lastly, note that the dissolution of β-$NaVO_3$ in water gives dihydrate species, $NaVO_3{\cdot}(2H_2O)$ that transform, above *ca.* 34 °C, to β-$NaVO_3$.[31,37] The irreversible transformation of β-$NaVO_3$ to α-$NaVO_3$ was reported to occur at 403–405 °C.[30]

The Raman spectrum of **1**$_{(500\text{-air})}$ features a characteristic sharp peak at 1039 cm^{-1} owing to the vanadium oxo stretching vibration[29,33,38,39] that is significantly reduced in intensity in β-$NaVO_3$/**1**$_{(500\text{-air})}$ and α-$NaVO_3$/**1**$_{(500\text{-air})}$ (Fig. 1a and S1†). The latter materials contain also bands of β-$NaVO_3$ and α-$NaVO_3$ at 945 and 954 cm^{-1}, respectively, but with diverging intensities. The characteristic Raman band of β-$NaVO_3$ is minor and the band of α-$NaVO_3$ is major in β-$NaVO_3$/**1**$_{(500\text{-air})}$. In α-$NaVO_3$/**1**$_{(500\text{-air})}$, the band of β-$NaVO_3$ is more intense than the band of α-$NaVO_3$, although both bands are less intense than in β-$NaVO_3$/**1**$_{(500\text{-air})}$. In addition, two broad peaks at 804 and 737 cm^{-1} that match the peak positions in the $Na_{1+x}V_3O_8/SiO_{2(500\text{-air})}$ reference are observed in β-$NaVO_3$/**1**$_{(500\text{-air})}$ and, to a larger extent, in α-$NaVO_3$/**1**$_{(500\text{-air})}$ (Fig. 1a).[29] In this $Na_{1+x}V_3O_8/SiO_{2(500\text{-air})}$ material, the $Na_{1+x}V_3O_8$ phase interacts with the SiO_2 support, as evidenced by Raman, ^{51}V and ^{23}Na NMR data, although the exact nature of the formed sites is currently unclear.[29] The Raman peaks at 804 and 737 cm^{-1} in α-$NaVO_3$/**1**$_{(500\text{-air})}$ are more intense in comparison to β-$NaVO_3$/**1**$_{(500\text{-air})}$, probably due to the lower dispersion and increased long-range order of the $Na_{1+x}V_3O_8$ phase in α-$NaVO_3$/**1**$_{(500\text{-air})}$; besides, the β-$NaVO_3$ peak has a lower intensity in β-$NaVO_3$/**1**$_{(500\text{-air})}$. Considering that α-$NaVO_3/SiO_{2(500\text{-air})}$ (*i.e.* the catalyst made

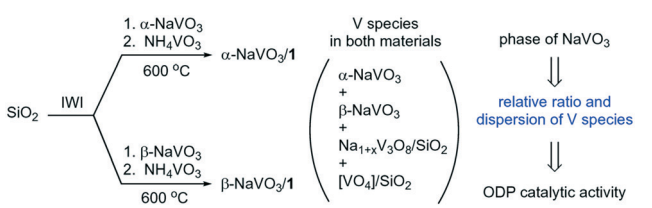

Scheme 1 Silica-supported materials and vanadium species prepared in this work. (IWI stands for incipient wetness impregnation).

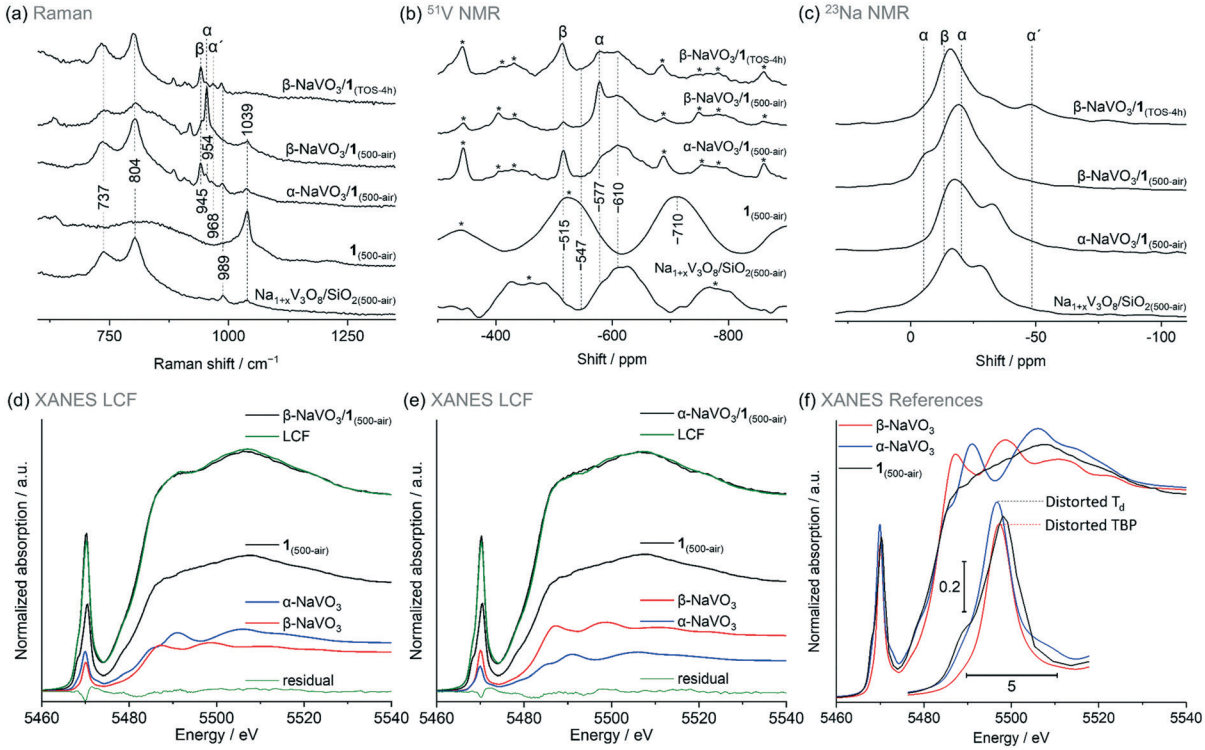

Fig. 1 (a) Raman, (b) ^{51}V and (c) ^{23}Na MAS NMR spectra of the studied materials (see labels in the panels); (d) and (e) are linear combination fittings (LCF, see Table 1 for details) of the V K-edge XANES of α-$NaVO_3$/**1** and β-$NaVO_3$/**1** dehydroxylated at 500 °C as well as f) V K-edge XANES spectra of the reference materials. Subscript TOS in hours indicates a used catalyst that was cooled down to room temperature while flowing the ODP gas mixture and handled in pristine conditions. Side bands of the NMR spectra are marked by asterisks; a spinning rate of 15–18 kHz was used. Notations α, β, and α′ indicate α-$NaVO_3$, β-$NaVO_3$ and α′-NaV_2O_5 phases, respectively. Characterization of $Na_{1+x}V_3O_8/SiO_{2(500\text{-air})}$ was reported by us previously and is reproduced here for comparison purposes.[29]

by IWI of α-$NaVO_3$ on silica at a nominal vanadium loading of 1 V nm^{-2}) does not feature peaks at 804 and 737 cm^{-1},[29] these bands must have been formed owing to an interaction between $[VO_4]/SiO_2$ and α-/β-$NaVO_3$. These species may feature different degrees of dispersion and/or crystallinity, which leads to different intensities in Raman spectra (*vide infra*).[33,40]

It is conceivable that the melting of α-$NaVO_3$ on the SiO_2 surface upon calcination and its subsequent recrystallization during cooling yielded the metastable β-$NaVO_3$ polymorph, owing to the more favorable interaction of this polymorph with the V-based, supported species. To test this hypothesis, we calcined α-$NaVO_3$/**1** to *ca.* 600 °C *in situ* in a Raman cell (Linkam CCR1000) under flow of synthetic air (30 ml min^{-1}). By recording spectra from the various regions of the specimen heated to *ca.* 600 °C and then cooled down to room temperature, we observed an inhomogeneous distribution of vanadium species, which is possibly related to heat transfer gradients in the *in situ* Raman cell. Specifically, two distinct areas were found, *viz.* areas with peaks of α-$NaVO_3$ and isolated vanadyl sites, as well as areas containing predominantly peaks of β-$NaVO_3$ and $Na_{1+x}V_3O_8/SiO_2$ (beam spot size was *ca.* 1.6 μm, Fig. S2†). In a control experiment, calcination of α-$NaVO_3$/**1** in a muffle furnace at 600 °C for 4 h with the subsequent exposure to air gave a more homogeneous material that predominately features peaks of β-$NaVO_3$ and $Na_{1+x}V_3O_8$; only occasionally areas with α-$NaVO_3$ and $[VO_4]$ sites are found (Fig. S3†). These experiments suggest that α-$NaVO_3$ may react with $[VO_4]/SiO_2$ to give $Na_{1+x}V_3O_8/SiO_2$ and β-$NaVO_3$. This mechanism for the formation of metastable β-$NaVO_3$ does not necessarily require recrystallization of the molten $NaVO_3$. Indeed, a differential scanning calorimetry (DSC) experiment of the calcination of α-$NaVO_3$/**1** reveals no clear features due to melting and recrystallization (Fig. S4†).

^{51}V magic angle spinning (MAS) NMR spectra of β-$NaVO_3$, α-$NaVO_3$, and $\mathbf{1}_{(500\text{-air})}$ give signals at −515, −577, and −710 ppm, respectively. In the ^{23}Na NMR spectrum of β-$NaVO_3$, one peak is observed *ca.* −13 ppm while two signals centered at −5 and −20 ppm are observed for α-$NaVO_3$ (Fig. 1b and S5†).[11,29,36,41] In line with Raman spectroscopy results, peaks due to β- and α-$NaVO_3$ are observed in the ^{51}V NMR spectra of α-$NaVO_3$/$\mathbf{1}_{(500\text{-air})}$ and β-$NaVO_3$/$\mathbf{1}_{(500\text{-air})}$; the signal from β-$NaVO_3$ is more intense for α-$NaVO_3$/$\mathbf{1}_{(500\text{-air})}$. A broad feature at *ca.* −610 ppm is observed for both promoted catalysts and $Na_{1+x}V_3O_8/SiO_{2(500\text{-air})}$. At least in part, this broad feature may be due to the vanadyl sites interacting with a Na^+ cation, which induces a downfield shift by 100 ppm compared to that in $\mathbf{1}_{(500\text{-air})}$ (Fig. 1b).[26,28,29] Note that a broad shoulder at the same position of *ca.* −610 ppm is also

observed for α-$NaVO_3$/$SiO_{2(500\text{-air})}$, and it is likely due to a partial decomposition of silica-supported α-$NaVO_3$ to vanadyl sites interacting with the nearby sodium cations on surface siloxides ($(-O)_3V{=}O\cdots Na^+$, Fig. S6†). Consistent with our inferences from the Raman and ^{51}V NMR data, ^{23}Na MAS NMR of the promoted catalysts shows peaks that can be ascribed to α-, β-$NaVO_3$, and $Na_{1+x}V_3O_8/SiO_2$ species (Fig. 1c). Interestingly, the feature due to β-$NaVO_3$ centered at −13 ppm is more prominent in α-$NaVO_3$/$\mathbf{1}_{(500\text{-air})}$ while two features due to α-$NaVO_3$ (centered at −21 and −5 ppm) are more prominent in β-$NaVO_3$/$\mathbf{1}_{(500\text{-air})}$ and are not noticeable in α-$NaVO_3$/$\mathbf{1}_{(500\text{-air})}$. ^{23}Na MAS NMR spectra of $Na_{1+x}V_3O_8/SiO_{2(500\text{-air})}$ and α-$NaVO_3$/$\mathbf{1}_{(500\text{-air})}$ are similar, with a *ca.* 5 ppm upfield shift of peaks in the latter material. This indicates that $Na_{1+x}V_3O_8/SiO_2$ is a major phase in α-$NaVO_3$/$\mathbf{1}_{(500\text{-air})}$ and that this material has nearly no Na atoms in the environment of α-$NaVO_3$. Features of $Na_{1+x}V_3O_8/SiO_2$ are less prominent in β-$NaVO_3$/$\mathbf{1}_{(500\text{-air})}$ (assessed by the peak at −28 ppm) and this is offset by more intense features of α- and β-$NaVO_3$.

The intensity of the pre-edge peak in V K-edge XANES depends on the symmetry of the ligand sphere around the vanadium atom such that a more centro-symmetric environment gives lower pre-edge peak heights in the order: tetrahedral (T_d) > distorted tetrahedral > square pyramidal (SP) > distorted octahedral (O_h) > octahedral (O_h, Fig. S7†).[17,29,42] The spectra of $\mathbf{1}_{(\text{air-500})}$ is consistent with V sites in a T_d coordination.[29] The V K-edge XANES spectra of $Na_{1+x}V_3O_8/SiO_2$ and **1** (exposed to air or dehydroxylated) are similar (Fig. S8 and S9†), indicating structural similarities of the V sites in those materials. To quantify the different V species present in the promoted materials we used linear combination fitting (LCF) of the V K-edge XANES spectra of the α- and β-$NaVO_3$/$\mathbf{1}_{(500\text{-air})}$. In this analysis, we used the well-defined material $\mathbf{1}_{(\text{air-500})}$ as one of the references, as well as α-$NaVO_3$ and β-$NaVO_3$. LCF analysis yielded a slightly higher fraction of α-$NaVO_3$ than β-$NaVO_3$ in β-$NaVO_3$/$\mathbf{1}_{(500\text{-air})}$ (24 and 20%, respectively, Table 1, entry 1) and a moderately higher fraction of β-$NaVO_3$ in α-$NaVO_3$/$\mathbf{1}_{(500\text{-air})}$ in comparison to α-$NaVO_3$ (28 and 16%, respectively, Table 1, entry 2, and Fig. 1d–f). These obtained phase percentages are consistent with the Raman and MAS NMR observations described above. Similar values for $\mathbf{1}_{(500\text{-air})}$ were obtained for both promoted materials (56%).

To investigate the dispersion of the α-$NaVO_3$, β-$NaVO_3$ and $Na_{1+x}V_3O_8/SiO_{2(500\text{-air})}$ phases in α-$NaVO_3$/$\mathbf{1}_{(500\text{-air})}$ and β-$NaVO_3$/$\mathbf{1}_{(500\text{-air})}$, Raman maps were collected. The freshly calcined materials were sealed in quartz capillaries under an inert atmosphere and Raman maps acquired from in total 225 points (15 × 15) separated by 4 μm (the laser spot size was *ca.* 1.6 μm). The intensities of the characteristic Raman peaks at 954, 945, 804 cm^{-1} (±2 cm^{-1}) were used to map α-$NaVO_3$, β-$NaVO_3$, and $Na_{1+x}V_3O_8/SiO_2$, respectively (Fig. 2a and S10†). We observe that α-$NaVO_3$ is less uniformly dispersed than β-$NaVO_3$ in α-$NaVO_3$/$\mathbf{1}_{(500\text{-air})}$ or β-$NaVO_3$/$\mathbf{1}_{(500\text{-air})}$. In addition, $Na_{1+x}V_3O_8/SiO_2$ appears more abundant and less well dispersed in α-$NaVO_3$/$\mathbf{1}_{(500\text{-air})}$ relative to β-$NaVO_3$/$\mathbf{1}_{(500\text{-air})}$. Yet for both promoted materials, the distribution of the intensities of β-$NaVO_3$ and $Na_{1+x}V_3O_8/SiO_2$ in the Raman maps is relatively similar, *i.e.* these phases are found similarly dispersed, which suggests an interaction between these two phases. Furthermore, EDX mapping of β-$NaVO_3$/**1** and α-$NaVO_3$/**1** (exposed to air during the sample transfer) shows a more uniform dispersion of Na and V in β-$NaVO_3$/**1** compared to α-$NaVO_3$/**1** that shows agglomerates of a Na/V rich phase (Fig. 2b).

The reducibility of supported vanadium-based catalysts for the oxidative dehydrogenation of propane and methanol (with vanadium loading below the monolayer coverage) was previously correlated with the turn over frequency (TOF) of those catalysts, such that higher reducibility is typically associated with higher activity.[6,43,44] However, a counter example is crystalline V_2O_5 on Al_2O_3 promoted with molybdenum that showed higher conversions and selectivities in ODP with decreasing reducibility of vanadium, as assessed by the temperature corresponding to the maximum of H_2 consumption (T_{max}) in the H_2 temperature-programmed reduction (TPR) experiment.[45] This indicates that the activity and selectivity of the V-based catalysts for ODP does not depend solely on their reducibility[6,43] but is influenced by other factors, for instance, the interaction with the support,[20,43] dispersion of the active phase,[29,46,47] V–O binding energy,[45] and acid–base properties.[48]

Considering that α-$NaVO_3$/**1** and β-$NaVO_3$/**1** contain similar species, but show distinct catalytic activity (*vide infra*), we were interested to compare H_2-TPR profiles of these two catalysts. A slightly lower T_{max} was observed for the more active catalyst, β-$NaVO_3$/**1**, as compared to α-$NaVO_3$/**1** (555 and 580 °C, respectively, Fig. S11†), while T_{max} of the less active $Na_{1+x}V_3O_8/SiO_2$ and **1** catalysts were centered at 602 and 473 °C, consistent with the different nature of vanadium species in studied catalysts.

In summary, Raman spectroscopy, ^{51}V and ^{23}Na MAS NMR data as well as LCF of XANES spectra show that α- and β-$NaVO_3$ as well as $Na_{1+x}V_3O_8$ interacting with the silica support are present in α-$NaVO_3$/$\mathbf{1}_{(500\text{-air})}$ and β-$NaVO_3$/$\mathbf{1}_{(500\text{-air})}$ materials, albeit in different relative amounts. The dispersion of Na and V species is higher in β-$NaVO_3$/$\mathbf{1}_{(500\text{-air})}$ compared to α-$NaVO_3$/$\mathbf{1}_{(500\text{-air})}$ according to Raman and EDX mapping. By NMR and Raman spectroscopies, a higher fraction of $Na_{1+x}V_3O_8/SiO_2$ and β-$NaVO_3$ is found in α-$NaVO_3$/$\mathbf{1}_{(500\text{-air})}$ relative to β-$NaVO_3$/$\mathbf{1}_{(500\text{-air})}$. The unexpected formation of the metastable β-$NaVO_3$ polymorph from the thermodynamically

Table 1 Linear combination fitting (LCF) results of the V K-edge XANES spectra of the promoted catalysts

Entry	Material	β-$NaVO_3$	α-$NaVO_3$	$\mathbf{1}_{(500\text{-air})}$[a]
1	β-$NaVO_3$/$\mathbf{1}_{(500\text{-air})}$	20	24	56
2	α-$NaVO_3$/$\mathbf{1}_{(500\text{-air})}$	28	16	56
3	β-$NaVO_3$/$\mathbf{1}_{(\text{TOS-4h})}$	28	21	51

[a] Representing $Na_{1+x}V_3O_8/SiO_{2(500\text{-air})}$ (see Fig. S8 and S9†).

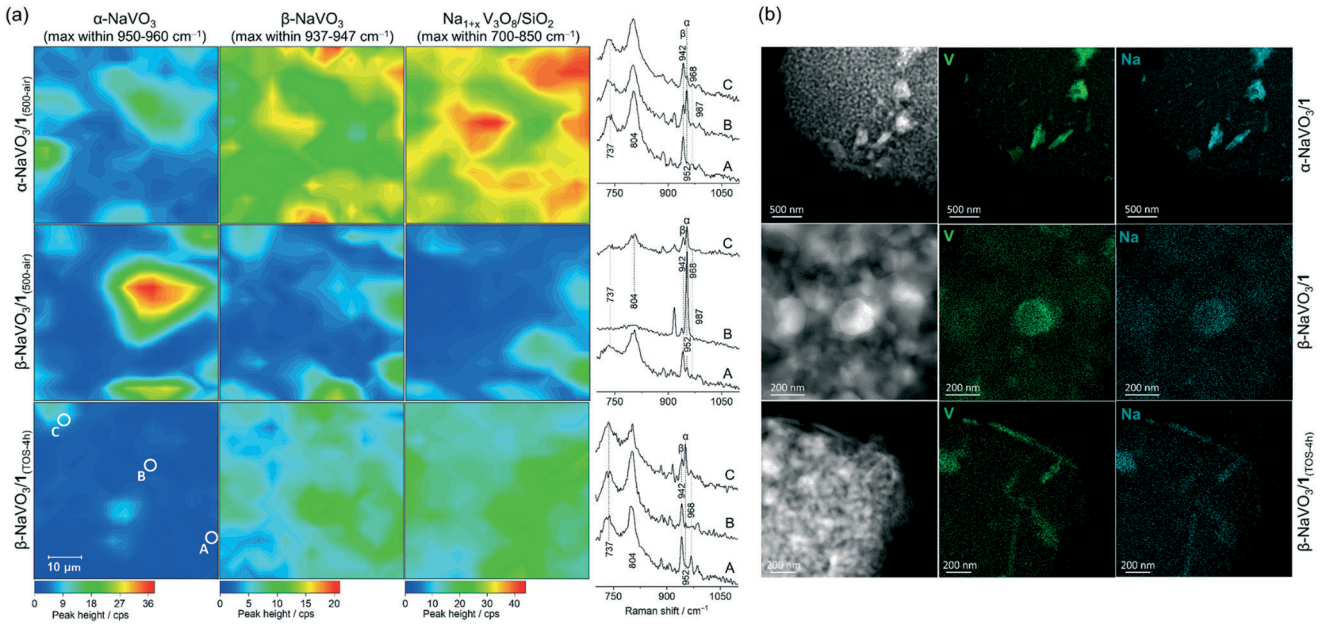

Fig. 2 (a) Raman mapping of α-$NaVO_3$/**1**$_{(500\text{-air})}$, β-$NaVO_3$/**1**$_{(500\text{-air})}$ and β-$NaVO_3$/**1**$_{(TOS\text{-}4h)}$ cooled down in an ODP atmosphere; the spectra shown correspond to the areas marked with A, B, and C (bottom left panel). (b) EDX mapping of α- and β-$NaVO_3$/**1** as well as β-$NaVO_3$/**1**$_{(TOS\text{-}4h)}$ (exposed to air).

stable α-$NaVO_3$ is likely due to the stabilizing interaction between β-$NaVO_3$ and $Na_{1+x}V_3O_8/SiO_2$ species, as compared to the respective interaction with α-$NaVO_3$. This is supported by the fact that the calcination of β-$NaVO_3$ on silica without vanadyl sites leads to α-$NaVO_3$ (Fig. S12†).[29] The materials $Na_{1+x}V_3O_8/SiO_2$ and α-$NaVO_3/SiO_{2(500\text{-air})}$ likely contain structurally similar $(-O)_3V{=}O\cdots Na^+$ sites, as suggested by the characteristic broad feature in the respective ^{51}V MAS NMR spectra at −610 ppm (Fig. 1b and S6a†). However, Raman bands at 737 and 804 cm^{-1} due to V–O–V bonds, diagnostic for $Na_{1+x}V_3O_8/SiO_{2(500\text{-air})}$, are not observed for α-$NaVO_3/SiO_{2(500\text{-air})}$.[17,29] Studies to refine our understanding of the nature of sites in $Na_{1+x}V_3O_8/SiO_2$ go beyond the scope of this work.

When the weight loadings of vanadium in the promoted catalysts were similar to that of the benchmark catalyst **1** (*ca.* 2 wt%, Na/V = 0.6), a higher initial specific activity was obtained for α- and β-$NaVO_3$/**1** catalysts (3.4 and 5.7 mmol C_3H_6 mol V^{-1} s^{-1}) than for **1** (2.5 mmol C_3H_6 mol V^{-1} s^{-1}), albeit the propene selectivities of α-$NaVO_3$/**1** and β-$NaVO_3$/**1** (64 and 59%) were lower than of **1** (74%, Fig. 3a). Yet α-$NaVO_3$/**1** and β-$NaVO_3$/**1** deactivate with TOS, after 4 h by 12 and 21%, respectively. However, the specific activity of α-$NaVO_3$/**1**$_{(0.7V)}$ and β-$NaVO_3$/**1**$_{(0.7V)}$, *i.e.* materials with a similar vanadium surface density to that of **1** (*ca.* 1.1 V nm^{-2} obtained at *ca.* Na/V ratio of 0.3, Table S1†) were 2.5 and 3.5 mmol C_3H_6 mol V^{-1} s^{-1}, respectively, while a similar selectivity of 74% was observed for all three these catalysts. Noteworthy, α-$NaVO_3$/**1**$_{(0.7V)}$ and β-$NaVO_3$/**1**$_{(0.7V)}$ did not deactivate with TOS after 240 min (at *ca.* 2.9 and 4.0% conversion, respectively, Fig. S14†). These results demonstrate that the surface density of Na and V influence catalyst activity, selectivity and stability.

By increasing the contact time, the conversion increases, yet the selectivity of the benchmark catalyst (**1**) drops with a higher rate compared to both promoted catalysts (Fig. 3b). For a nominal V loading of 1 V nm^{-2}, the benchmark catalyst **1** shows a higher selectivity to propene compared to the promoted catalysts at similar conversions that did not exceed 8% (Fig. 3b). Our promoted catalysts show higher propene selectivities at conversions exceeding 10%, *i.e.* 58, 51 and 41% at 13, 15 and 13% propane conversion for β-$NaVO_3$/**1**, α-$NaVO_3$/**1** and **1**, respectively (Fig. S13†). Overall, these values translate into higher initial productivities (within 30 min) for the promoted catalysts relative to **1**.

Furthermore, the productivity of β-$NaVO_3$/**1** is *ca.* 2.4 times higher than that of **1** at similar propane conversion (0.39 *vs.* 0.16 kg_{C3H6} kg_{cat}^{-1} h^{-1} at 4.7 *vs.* 4.3%, respectively, Fig. 3b). Interestingly, $Na_{1+x}V_3O_8/SiO_2$ showed the highest initial selectivity to propene among the studied catalysts, reaching 80% at a 2.2% propane conversion, *i.e.* slightly higher than the sodium-free benchmark catalyst **1** (77% at 3.6% propane conversion at 450 °C). In addition to propene, $Na_{1+x}V_3O_8/SiO_2$ and **1** produced up to *ca.* 3% C_2H_4 while α-$NaVO_3$/**1** and β-$NaVO_3$/**1** only gave propene and CO_x, with an initial propene selectivity of 64 and 59% at 5.8 and 8.2% conversions, respectively. At similar reaction conditions (WHSV = 6.8 h^{-1}), the $Na_6V_{10}O_{28}/SiO_2$ catalyst reported by us previously[29] showed 65% propene selectivity at 6% propane conversion.

Notably, while the ODP activities of catalysts **1** and $Na_{1+x}V_3O_8/SiO_2$ are stable (Fig. S15,† typical for V-based ODP catalysts),[29] the catalytic activity of both promoted materials decreases with TOS (Fig. 3c). We observe a decline of the specific activity by 12 and 21% within 4 h TOS for α-$NaVO_3$/**1**

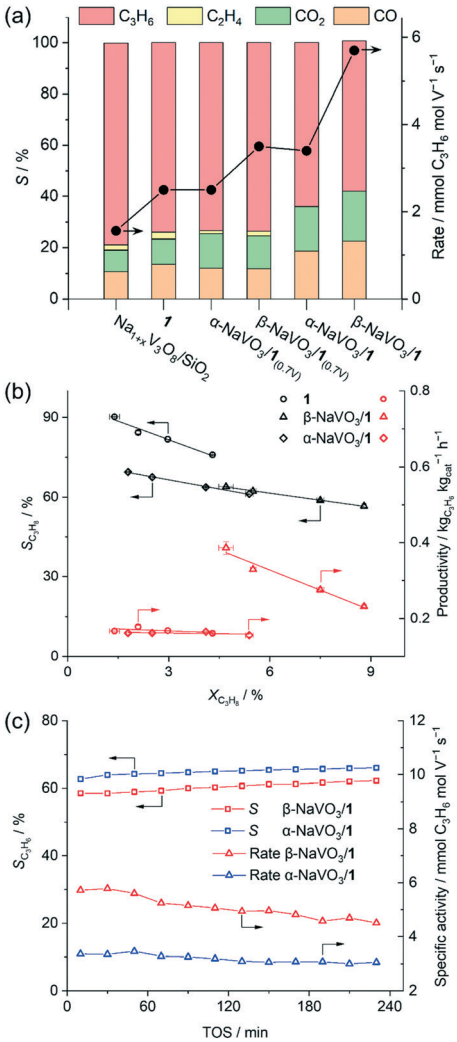

Fig. 3 (a) Initial catalytic activity (TOS = 30 min), (b) propene selectivity and productivity *vs.* propane conversion for the studied catalysts (see Table S1†). WHSV was varied between 5.1–13.6 h^{-1} by changing the total feed flow (15.8–42 ml min^{-1}). (c) Changes with TOS of β- and α-$NaVO_3$/**1** under ODP conditions (C_3H_8: air = 2: 5, total flow of 21 ml min^{-1}, 450 °C).

and β-$NaVO_3$/**1**, respectively. Comparison of the TEM images and EDX mapping of β-$NaVO_3$/**1** after 4 h TOS to the fresh catalyst reveals agglomeration of the Na and V species on the silica surface after the ODP reaction, which is a likely reason for deactivation (Fig. 2b). The Raman spectrum of the reacted β-$NaVO_3$/**1** (denoted β-$NaVO_3$/$\mathbf{1}_{(TOS\text{-}4h)}$; the material was handled without exposure to air) shows a tangible increase in the intensity of the peaks at 737 and 804 cm^{-1} compared to the fresh catalyst. This can indicate the formation of a less dispersed $Na_{1+x}V_3O_8$ phase compared to the fresh catalyst and would be in line with the TEM analysis. The formation of three-dimensional V_2O_5 crystals has been reported to deactivate VO_x-based ODP catalysts.[6,20] Furthermore, the strongly reduced intensity of the 954 cm^{-1} peak of α-$NaVO_3$ might be due to its reaction with [VO_4] sites and transformation to $Na_{1+x}V_3O_8/SiO_2$ with TOS that decrease the number of active sites (possibly, $(-O)_3V{=}O\cdots Na^+$ sites). That being said, no notable change was observed in the characteristic peak of β-$NaVO_3$ (945 cm^{-1}, Fig. 1a). In addition, a low-intensity peak at 968 cm^{-1} due to α′-NaV_2O_5 is also observed in β-$NaVO_3$/$\mathbf{1}_{(TOS\text{-}4h)}$ (Fig. 1a). Note that we have previously shown that α′-NaV_2O_5 forms on the silica surface under inert conditions owing to the reaction between β-$NaVO_3$ and $Na_{1+x}V_3O_8/SiO_2$; α′-NaV_2O_5 is poorly active for ODP.[29] In agreement with the Raman data, ^{51}V MAS NMR of β-$NaVO_3$/$\mathbf{1}_{(TOS\text{-}4h)}$ shows a decreased intensity of α-$NaVO_3$ signatures and an increased intensity of β-$NaVO_3$ that also broadens (Fig. 1b).[49] MAS NMR data on ^{23}Na nucleus shows a new peak centered at −48 ppm for β-$NaVO_3$/$\mathbf{1}_{(TOS\text{-}4h)}$, due to the formation of the α′-NaV_2O_5 phase. A decreased intensity of the α-$NaVO_3$ phase (peaks at −21 and −5 ppm, Fig. 1c) is also observed.

We discussed above that Raman mapping of β-$NaVO_3$/$\mathbf{1}_{(500\text{-}air)}$ shows inhomogeneous distribution of α-$NaVO_3$ in this material, while β-$NaVO_3$ and $Na_{1+x}V_3O_8/SiO_2$ are more homogeneously dispersed compared to α-$NaVO_3$ (Fig. 2a). After 4 h TOS, *i.e.* β-$NaVO_3$/$\mathbf{1}_{(TOS\text{-}4h)}$, Raman peaks of the α-$NaVO_3$ phase have decreased notably, while peaks of β-$NaVO_3$ and $Na_{1+x}V_3O_8/SiO_2$ phases have increased (Fig. 2a). As mentioned, this might be due to a reaction of the remaining vanadyl sites on silica with α-$NaVO_3$ forming crystalline (three-dimensional) $Na_{1+x}V_3O_8$ that is associated with a decreased catalytic activity. Raman maps in Fig. 2a also show that the increased intensity of signals related to $Na_{1+x}V_3O_8/SiO_2$ correlates with an increased intensity of the β-$NaVO_3$ peak, which is consistent with the aforementioned hypothesis of an increased stabilization of the metastable β-$NaVO_3$ by $Na_{1+x}V_3O_8/SiO_2$, in preference to the formation of α-$NaVO_3$, which is consumed with TOS in β-$NaVO_3$/$\mathbf{1}_{(500\text{-}air)}$ (Fig. 2a).

Conclusions

[VO_4]/SiO_2 promoted with α- or β-polymorphs of $NaVO_3$ shows an increase in the initial rate of propene formation for ODP by 30 and 125%, respectively, at similar vanadium loadings (*ca.* 1 V nm^{-2} nominal coverage and 2 wt%), albeit offset by a 10 and 15% decrease in propene selectivity. Both catalysts lose activity with TOS due to the agglomeration and formation of less well dispersed (and possibly crystalline) $Na_{1+x}V_3O_8$. Calcination of vanadyl sites promoted by β-$NaVO_3$ leads to the α-$NaVO_3$ phase, while promotion of vanadyl sites with α-$NaVO_3$ gives notable amounts of the β-$NaVO_3$ phase, which is unexpected considering that β-$NaVO_3$ (both bulk and silica-supported) transforms completely to α-$NaVO_3$ already at *ca.* 400 °C. The stabilization of the metastable β-$NaVO_3$ on [VO_4]/SiO_2 is associated with the formation of dispersed $Na_{1+x}V_3O_8$ that interacts with the silica support. The interaction of [VO_4]/SiO_2 with β-$NaVO_3$ seems to lead to $Na_{1+x}V_3O_8$ with a higher dispersion on silica than when promoted by α-$NaVO_3$, resulting in a higher catalytic activity for the β-$NaVO_3$ promoted catalyst. We are currently exploring

other ways (such as support effect) to maintain a high dispersion of $Na_{1+x}V_3O_8$.

Conflicts of interest

There are no conflicts to declare.

Acknowledgements

We gratefully acknowledge the Scientific Centre for Optical and Electron Microscopy (ScopeM) of ETH Zürich for providing access to electron microscopes. The Paul Scherer Institute (PSI), SuperXAS beamline is acknowledged for providing access to the synchrotron X-ray facility.

Notes and references

1 J. S. Plotkin, The changing dynamics of olefin supply/demand, *Catal. Today*, 2005, **106**, 10–14.
2 J. J. H. B. Sattler, J. Ruiz-Martinez, E. Santillan-Jimenez and B. M. Weckhuysen, Catalytic Dehydrogenation of Light Alkanes on Metals and Metal Oxides, *Chem. Rev.*, 2014, **114**, 10613–10653.
3 E. McFarland, Unconventional Chemistry for Unconventional Natural Gas, *Science*, 2012, **338**, 340–342.
4 J. T. Grant, J. M. Venegas, W. P. McDermott and I. Hermans, Aerobic Oxidations of Light Alkanes over Solid Metal Oxide Catalysts, *Chem. Rev.*, 2018, **118**, 2769–2815.
5 M. M. Bhasin, J. H. McCain, B. V. Vora, T. Imai and P. R. Pujadó, Dehydrogenation and oxydehydrogenation of paraffins to olefins, *Appl. Catal., A*, 2001, **221**, 397–419.
6 C. A. Carrero, R. Schloegl, I. E. Wachs and R. Schomaecker, Critical Literature Review of the Kinetics for the Oxidative Dehydrogenation of Propane over Well-Defined Supported Vanadium Oxide Catalysts, *ACS Catal.*, 2014, **4**, 3357–3380.
7 Y. Wang, H. Su, Y. Gu, X. Song and J. Zhao, Carcinogenicity of chromium and chemoprevention: a brief update, *OncoTargets Ther.*, 2017, **10**, 4065–4079.
8 R. R. Langeslay, D. M. Kaphan, C. L. Marshall, P. C. Stair, A. P. Sattelberger and M. Delferro, Catalytic Applications of Vanadium: A Mechanistic Perspective, *Chem. Rev.*, 2019, **119**, 2128–2191.
9 H. Eckert, G. Deo, I. E. Wachs and A. M. Hirt, Solid state ^{51}V NMR structural studies of vanadium(V) oxide catalysts supported on TiO_2 (anatase) and TiO_2 (rutile). The influence of surface impurities on the vanadium(V) coordination, *Colloids Surf.*, 1990, **45**, 347–359.
10 O. B. Lapina, V. M. Mastikhin, L. G. Simonova and Y. O. Bulgakova, Characterization of surface species of supported V_2O_5-Al_2O_3 catalysts by ^{51}V NMR, *J. Mol. Catal.*, 1991, **69**, 61–73.
11 N. Das, H. Eckert, H. Hu, I. E. Wachs, J. F. Walzer and F. J. Feher, Bonding states of surface vanadium(V) oxide phases on silica: structural characterization by vanadium-51 NMR and Raman spectroscopy, *J. Phys. Chem.*, 1993, **97**, 8240–8243.
12 N. R. Jaegers, J.-K. Lai, Y. He, E. Walter, D. A. Dixon, M. Vasiliu, Y. Chen, C. Wang, M. Y. Hu, K. T. Mueller, I. E. Wachs, Y. Wang and J. Z. Hu, Mechanism by which Tungsten Oxide Promotes the Activity of Supported V_2O_5/TiO_2 Catalysts for NO_X Abatement: Structural Effects Revealed by ^{51}V MAS NMR Spectroscopy, *Angew. Chem., Int. Ed.*, 2019, **58**, 12609–12616.
13 N. R. Jaegers, C. Wan, M. Y. Hu, M. Vasiliu, D. A. Dixon, E. Walter, I. E. Wachs, Y. Wang and J. Z. Hu, Investigation of Silica-Supported Vanadium Oxide Catalysts by High-Field ^{51}V Magic-Angle Spinning NMR, *J. Phys. Chem. C*, 2017, **121**, 6246–6254.
14 T. Tanaka, H. Yamashita, R. Tsuchitani, T. Funabiki and S. Yoshida, X-ray absorption (EXAFS/XANES) study of supported vanadium oxide catalysts. Structure of surface vanadium oxide species on silica and γ-alumina at a low level of vanadium loading, *J. Chem. Soc., Faraday Trans.*, 1988, **84**, 2987–2999.
15 E. L. Lee and I. E. Wachs, In Situ Raman Spectroscopy of SiO_2-Supported Transition Metal Oxide Catalysts: An Isotopic ^{18}O–^{16}O Exchange Study, *J. Phys. Chem. C*, 2008, **112**, 6487–6498.
16 S. T. Oyama, G. T. Went, K. B. Lewis, A. T. Bell and G. A. Somorjai, Oxygen chemisorption and laser Raman spectroscopy of unsupported and silica-supported vanadium oxide catalysts, *J. Phys. Chem.*, 1989, **93**, 6786–6790.
17 X. Gao, S. R. Bare, B. M. Weckhuysen and I. E. Wachs, In Situ Spectroscopic Investigation of Molecular Structures of Highly Dispersed Vanadium Oxide on Silica under Various Conditions, *J. Phys. Chem. B*, 1998, **102**, 10842–10852.
18 X. Gao, M. A. Bañares and I. E. Wachs, Ethane and n-Butane Oxidation over Supported Vanadium Oxide Catalysts: An in Situ UV–Visible Diffuse Reflectance Spectroscopic Investigation, *J. Catal.*, 1999, **188**, 325–331.
19 X. Gao and I. E. Wachs, Investigation of Surface Structures of Supported Vanadium Oxide Catalysts by UV–vis–NIR Diffuse Reflectance Spectroscopy, *J. Phys. Chem. B*, 2000, **104**, 1261–1268.
20 C. A. Carrero, C. J. Keturakis, A. Orrego, R. Schomacker and I. E. Wachs, Anomalous reactivity of supported V_2O_5 nanoparticles for propane oxidative dehydrogenation: influence of the vanadium oxide precursor, *Dalton Trans.*, 2013, **42**, 12644–12653.
21 C. Carrero, M. Kauer, A. Dinse, T. Wolfram, N. Hamilton, A. Trunschke, R. Schlogl and R. Schomacker, High performance $(VO_x)n$-$(TiO_x)m$/SBA-15 catalysts for the oxidative dehydrogenation of propane, *Catal. Sci. Technol.*, 2014, **4**, 786–794.
22 J. T. Grant, C. A. Carrero, F. Goeltl, J. Venegas, P. Mueller, S. P. Burt, S. E. Specht, W. P. McDermott, A. Chieregato and I. Hermans, Selective oxidative dehydrogenation of propane to propene using boron nitride catalysts, *Science*, 2016, **354**, 1570–1573.
23 A. A. Lemonidou, L. Nalbandian and I. A. Vasalos, Oxidative dehydrogenation of propane over vanadium oxide based catalysts: Effect of support and alkali promoter, *Catal. Today*, 2000, **61**, 333–341.
24 G. Garcia Cortez, J. L. G. Fierro and M. A. Bañares, Role of potassium on the structure and activity of alumina-

supported vanadium oxide catalysts for propane oxidative dehydrogenation, *Catal. Today*, 2003, **78**, 219–228.

25 S. Takenaka, T. Tanaka, T. Yamazaki, T. Funabiki and S. Yoshida, Structure of Active Species in Alkali-Ion-Modified Silica-Supported Vanadium Oxide, *J. Phys. Chem. B*, 1997, **101**, 9035–9040.

26 J. T. Grant, A. M. Love, C. A. Carrero, F. Huang, J. Panger, R. Verel and I. Hermans, Improved supported metal oxides for the oxidative dehydrogenation of propane, *Top. Catal.*, 2016, **59**, 1545–1553.

27 S. Irusta, A. Marchi, E. Lombardo and E. Miré, Characterization of surface species on V/SiO_2 and $V, Na/SiO_2$ and their role in the partial oxidation of methane to formaldehyde, *Catal. Lett.*, 1996, **40**, 9–16.

28 J. T. Grant, C. A. Carrero, A. M. Love, R. Verel and I. Hermans, Enhanced Two-Dimensional Dispersion of Group V Metal Oxides on Silica, *ACS Catal.*, 2015, **5**, 5787–5793.

29 M. Nadjafi, P. M. Abdala, R. Verel, D. Hosseini, O. V. Safonova, A. Fedorov and C. R. Müller, Reducibility and Dispersion Influence the Activity in Silica-Supported Vanadium-Based Catalysts for the Oxidative Dehydrogenation of Propane: The Case of Sodium Decavanadate, *ACS Catal.*, 2020, **10**, 2314–2321.

30 I. Lukács and C. Strusievici, Über die Polymorphie von Natriummetavanadat, *Z. Anorg. Allg. Chem.*, 1962, **315**, 323–326.

31 S. Seetharaman, H. L. Bhat and P. S. Narayanan, Raman spectroscopic studies on sodium metavanadate, *J. Raman Spectrosc.*, 1983, **14**, 401–405.

32 I. E. Wachs, Catalysis science of supported vanadium oxide catalysts, *Dalton Trans.*, 2013, **42**, 11762–11769.

33 S. Xie, E. Iglesia and A. T. Bell, Effects of Hydration and Dehydration on the Structure of Silica-Supported Vanadia Species, *Langmuir*, 2000, **16**, 7162–7167.

34 A. M. Love, C. A. Carrero, A. Chieregato, J. T. Grant, S. Conrad, R. Verel and I. Hermans, Elucidation of Anchoring and Restructuring Steps during Synthesis of Silica-Supported Vanadium Oxide Catalysts, *Chem. Mater.*, 2016, **28**, 5495–5504.

35 K. C. Szeto, B. Loges, N. Merle, N. Popoff, A. Quadrelli, H. Jia, E. Berrier, A. De Mallmann, L. Delevoye, R. M. Gauvin and M. Taoufik, Vanadium Oxo Organometallic Species Supported on Silica for the Selective Non-oxidative Dehydrogenation of Propane, *Organometallics*, 2013, **32**, 6452–6460.

36 B. Schimmoeller, Y. Jiang, S. E. Pratsinis and A. Baiker, Structure of flame-made vanadia/silica and catalytic behavior in the oxidative dehydrogenation of propane, *J. Catal.*, 2010, **274**, 64–75.

37 K. Kato and E. Takayama, Das Entwasserungsverhalten des Natriummetavanadatdihydrats und die Kristallstruktur des β-Natriummetavanadats, *Acta Crystallogr., Sect. B: Struct. Sci.*, 1984, **40**, 102–105.

38 M. D. Argyle, K. Chen, A. T. Bell and E. Iglesia, Effect of Catalyst Structure on Oxidative Dehydrogenation of Ethane and Propane on Alumina-Supported Vanadia, *J. Catal.*, 2002, **208**, 139–149.

39 G. T. Went, S. T. Oyama and A. T. Bell, Laser Raman spectroscopy of supported vanadium oxide catalysts, *J. Phys. Chem.*, 1990, **94**, 4240–4246.

40 P. M. A. Sherwood, *Vibrational spectroscopy of solids*, CUP Archive, 1972.

41 J. Skibsted, N. C. Nielsen, H. Bildsoe and H. J. Jakobsen, Magnitudes and relative orientation of vanadium-51 quadrupole coupling and anisotropic shielding tensors in metavanadates and potassium vanadium oxide (KV_3O_8) from vanadium-51 MAS NMR spectra. Sodium-23 quadrupole coupling parameters for α- and β-$NaVO_3$, *J. Am. Chem. Soc.*, 1993, **115**, 7351–7362.

42 J. Wong, F. W. Lytle, R. P. Messmer and D. H. Maylotte, K-edge absorption spectra of selected vanadium compounds, *Phys. Rev. B: Condens. Matter Mater. Phys.*, 1984, **30**, 5596–5610.

43 A. Dinse, B. Frank, C. Hess, D. Habel and R. Schomäcker, Oxidative dehydrogenation of propane over low-loaded vanadia catalysts: Impact of the support material on kinetics and selectivity, *J. Mol. Catal. A: Chem.*, 2008, **289**, 28–37.

44 G. Deo and I. E. Wachs, Reactivity of Supported Vanadium Oxide Catalysts: The Partial Oxidation of Methanol, *J. Catal.*, 1994, **146**, 323–334.

45 S. Chen, L. Zeng, R. Mu, C. Xiong, Z.-J. Zhao, C. Zhao, C. Pei, L. Peng, J. Luo, L.-S. Fan and J. Gong, Modulating Lattice Oxygen in Dual-Functional Mo–V–O Mixed Oxides for Chemical Looping Oxidative Dehydrogenation, *J. Am. Chem. Soc.*, 2019, **141**, 18653–18657.

46 E. V. Kondratenko, N. Steinfeldt and M. Baerns, Transient and steady state investigation of selective and non-selective reaction pathways in the oxidative dehydrogenation of propane over supported vanadia catalysts, *Phys. Chem. Chem. Phys.*, 2006, **8**, 1624–1633.

47 P. Gruene, T. Wolfram, K. Pelzer, R. Schlögl and A. Trunschke, Role of dispersion of vanadia on SBA-15 in the oxidative dehydrogenation of propane, *Catal. Today*, 2010, **157**, 137–142.

48 I. Rossetti, G. F. Mancini, P. Ghigna, M. Scavini, M. Piumetti, B. Bonelli, F. Cavani and A. Comite, Spectroscopic Enlightening of the Local Structure Of VO_X Active Sites in Catalysts for the ODH of Propane, *J. Phys. Chem. C*, 2012, **116**, 22386–22398.

49 A. A. Zvyagin, Temperature dependence of the electron paramagnetic resonance linewidth in NaV_2O_5, *Phys. Rev. B*, 2001, **63**, 172409.